Ore Geology Reviews 139 (2021) 104534

Contents lists available at ScienceDirect

Ore Geology Reviews

journal homepage: www.elsevier.com/locate/oregeorev

Isotopic fingerprints of recycled eclogite facies sediments in the generation of the Huanglongpu carbonatite, central China

Xiao-Chen Zhao [a,b], Shuang Yan [a,c,*], He-Cai Niu [a,c], Qi-Bin Zhang [a,b,d], Xu Zhao [a,c], Jian Wu [a,e], Wu-Bin Yang [a,c]

[a] CAS Key Laboratory of Mineralogy and Metallogeny/Guangdong Provincial Key Laboratory of Mineral Physics and Materials, Guangzhou Institute of Geochemistry, Chinese Academy of Sciences, Guangzhou 510640, China
[b] University of Chinese Academy of Sciences, Beijing 100049, China
[c] CAS Center for Excellence in Deep Earth Science, Guangzhou 510640, China
[d] No.6 Institute of Geology and Mineral Resources Exploration of Shandong Province, China
[e] Nonferrous Metals Geological Bureau of Guangdong Province 932 Battalion, China

ARTICLE INFO

Keywords:
Carbonatite
Mo-REE mineralization
Calcite
Recycled eclogite facies sediments
Huanglongpu

ABSTRACT

Carbonatites are the most important sources of global niobium (Nb) and rare earth element (REE) resources, particularly the light REEs. The Huanglongpu carbonatite in central China is unique for the enrichment of molybdenum (Mo) and heavy REEs. Till now, the source nature of the Huanglongpu carbonatites is still poorly understood. In this contribution, we present elemental and C-O-Sr-Nd-Pb isotopic data of calcite to constrain the source signatures of the Huanglongpu carbonatite. Elemental geochemistry and C-O isotopes of the calcite vein-networks in the carbonatite reveal that the Huanglongpu carbonatites is of igneous genesis and originated from mantle-derived carbonatitic melts. The negative εNd(t) values (−8.03–−5.05) and elevated initial $^{87}Sr/^{86}Sr$ ratios (0.7049–0.7056) indicate considerable contribution of recycled crustal components in the mantle source. Combination of O-Sr-Nd-Pb isotopes suggests that over 10 wt% of recycled sediments might have been involved into the depleted mantle, accounting for the source of the Huanglongpu carbonatite. Considering the enrichment of heavy REE, REE distribution simulation indicates that the Huanglongpu carbonatite might be from the 30% partial melting of eclogite facies sediments. Accordingly, we infer that the Huanglongpu carbonatite might have been derived from the partial melting of a hybridized mantle source modified by recycled sediments of eclogite facies. The enrichment of Mo and heavy REEs plausibly resulted from the contribution of garnet/pyroxene from the eclogitic sediments within the subducted slab.

1. Introduction

Carbonatites have long been the important targets for critical metal explorations (e.g., Xu et al., 2008; Chen et al., 2018; Zhang et al., 2019a, b) as well as good lithoprobes to look into the crust-mantle interaction processes (e.g., Çimen et al., 2019). Carbonatites are usually characterized by light REEs (LREEs) enrichment and provide over 51.4% global LREE resources (e.g., Veksler et al., 1998; Song et al., 2015b), such as giant Bayan Obo REE-Fe-Nb deposit and the Maoniuping REE deposit in China, and the Mountain Pass REE deposit in USA (e.g., Lai and Yang, 2013; Ling et al., 2013; Liu et al., 2019). Besides, carbonatites are important mantle-derived igneous rocks that developed in the intraplate rifting settings (i.e., the East African carbonatites, Kalt et al., 1997; Benkóet al., 2021), anorogenic margins of craton (i.e., Bayan Obo and Maoniuping carbonatites, Fan et al., 2006; Hou et al., 2015; Liu et al., 2019; Weng et al., 2021), or mantle plumes (e.g., the Cape Verde islands, Gerlach et al., 1988). Even so, the origin of carbonatites has been long fascinated and subjected to several arguments. The Phanerozoic carbonatites (<200 Ma) in the East Africa were thought to originate from the mixture of the HIMU and EMI mantle components (e.g., Bell and Tilton, 2001). In some cases, carbonatites were considered to be generated due to partial melting of lithospheric mantle modified by recycled crustal components (e.g., Bell et al., 1982). The involvement of sediments into mantle source would not only lead to geochemical heterogeneity in the

* Corresponding author at: CAS Key Laboratory of Mineralogy and Metallogeny/Guangdong Provincial Key Laboratory of Mineral Physics and Materials, Guangzhou Institute of Geochemistry, Chinese Academy of Sciences, Guangzhou 510640, China.
E-mail address: yanshuang@gig.ac.cn (S. Yan).

https://doi.org/10.1016/j.oregeorev.2021.104534
Received 14 April 2021; Received in revised form 18 October 2021; Accepted 18 October 2021
Available online 23 October 2021

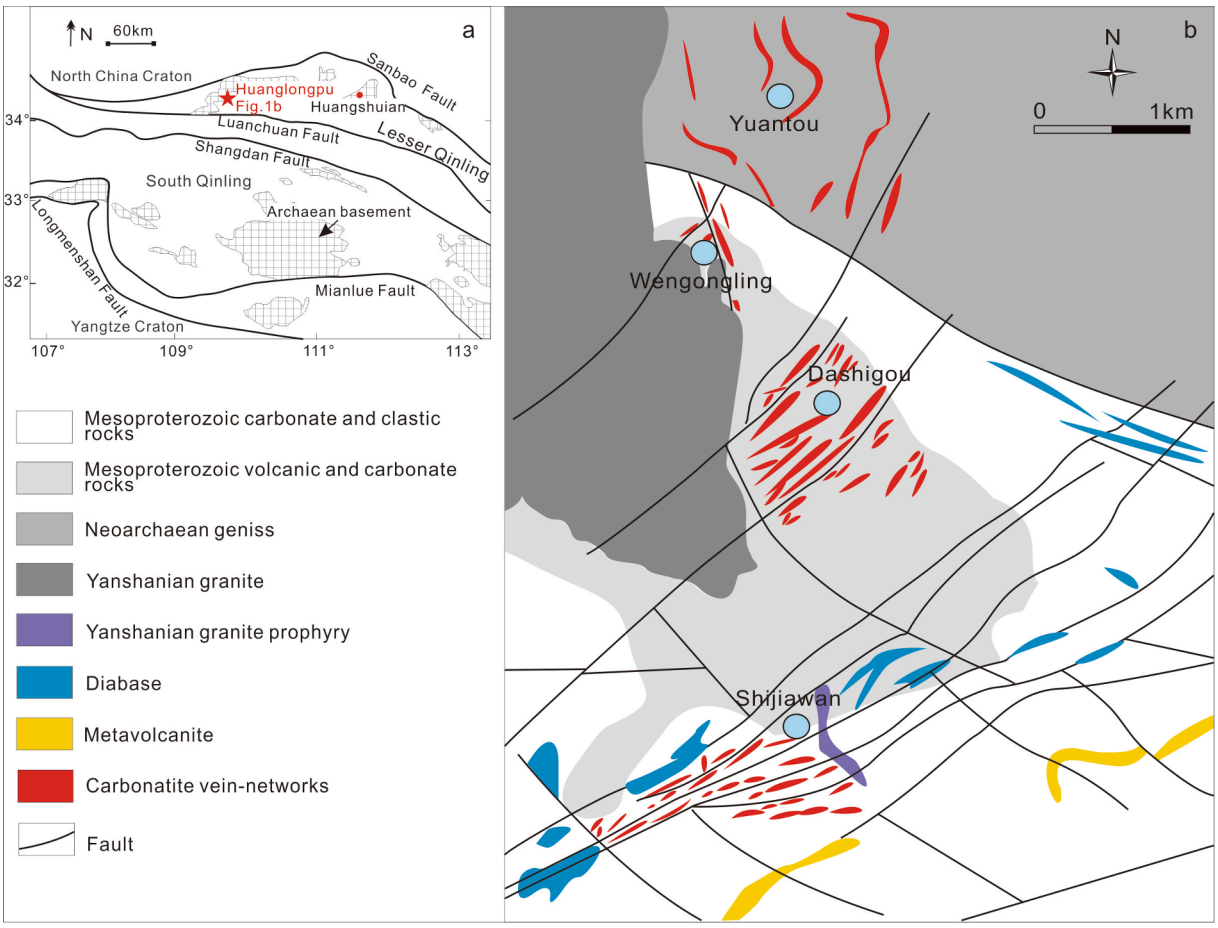

Fig. 1. (a) Tectonic subdivision of the Qingling Belt; and (b) Geological map of the Huanglongpu REE-Mo ore field. Modified after Xu et al. (2010).

mantle source, but also provides the precursor carbon and REEs for carbonatites (e.g., Hou et al., 2015; Weng et al., 2021).

The Huanglongpu deposit in Lesser Qinling, central China, is an Early Mesozoic carbonatite-type Mo-REE deposit (Bai et al., 2019; Smith et al., 2018; Xu et al., 2010), with molybdenite Re-Os age of 225.0 ± 7.6 Ma (Song et al., 2015a,b). Previous studies mostly focused on the REE (-Mo) mineralization mechanisms (i.e., Xu et al., 2010; Smith et al., 2018; Cangelosi et al., 2019) and the evolution process of the Huanglongpu carbonatites (Xu et al., 2007; Bai et al., 2019). Till now, the source nature of the unique Mo-HREE-bearing carbonatites is still not well constrained. In this paper, we conduct elemental and isotopic geochemistry of calcite from the carbonatites to decipher the source nature of the Huanglongpu carbonatites and origin of the Mo and HREE enrichments.

2. Geological background

The Qinling orogenic belt in central China, stretching 1500 km from east to west, lies between the North China Craton to the north and the Yangtze Craton to the south (Fig. 1a, Ratschbacher et al., 2003; Dong and Santosh, 2016). From south to north, the Qinling orogenic belt can be further subdivided into four parts, i.e., the northern margin of the Yangtze Craton, the South Qinling Belt, the North Qinling Belt and the southern margin of the North China Craton (the Lesser Qinling), separated by the Mianlue fault, Shangdan fault and Luanchuan fault, respectively (Fig. 1b, Chen and Santosh, 2014; Zhang et al., 2019a,b). The Qinling orogenic belt had experienced multi-stage tectonic evolution associated with the expansion and consumption of the Shangdan Ocean basin during the Cambrian to the Late Silurian and the Mianlue Ocean basin from the Devonian to the Middle Triassic (Lu et al., 1997; Chen and Santosh, 2014; Zhang et al., 2019a,b). During the Late Triassic, the closed Mianlue Ocean basin experienced extensional and collapsed after the orogenic period, forming numerous deep and large faults (Dong and Santosh, 2016; Zhang et al., 2019a,b).

The Huanglongpu Mo-HREE deposit is located in the Lesser Qinling (Fig. 1). The basement in the Lesser Qinling consists of the amphibolite- to granulite- facies metamorphic rocks of the Archean Taihua Group, which unconformably contacts with the metamorphic rocks and volcanic rocks of the Paleoproterozoic Xiong'er Group and is covered by the Proterozoic to Neoproterozoic sedimentary rocks (Huang et al., 2009). Faults in this region are mostly in northwest direction with 1–3 km in length. Mo-HREE mineralized carbonatites occur as veins and mesh-veins along the direction of the faults. The Huanglongpu ore field consists of several carbonatite-associated ore districts, including the Dashigou, Wengongling, Shijiawan, and Yuantou (Fig. 1c). They have similar mineral assemblages and compositional affinities with Mo-HREE mineralization. Over 200 kilotons of Mo with grades of 0.034 – 0.136 wt % and over 2 kilotons of rare earth elements reserves have been estimated in the Huanglongpu ore field (Xu et al., 2009).

Carbonatite samples in this study were collected from the Dashigou and Wengongling ore districts. Carbonatites are mostly present as vein-networks, 100–1000 m long and 0.1–20 m wide (Fig. 2a). Fresh and least altered carbonatite samples are mainly composed of calcite (>80 vol%), quartz, molybdenite, xenotime and monazite, with lesser pyrite, galena, sphalerite and REE-fluorocarbonate (Fig. 2b–f). Xenotime is the major HREE mineral in the Huanglongpu carbonatite. Molybdenite appears as thin films and is mainly distributed within carbonatites (Fig. 2b and e). Monazite U–Pb dating and molybdenite Re–Os dating of the Huanglongpu carbonatite indicated that the carbonatite and associated Mo-HREE mineralization took place at the Late Triassic (225 – 209 Ma), when the lesser Qinling was being in a post-collision extensional setting

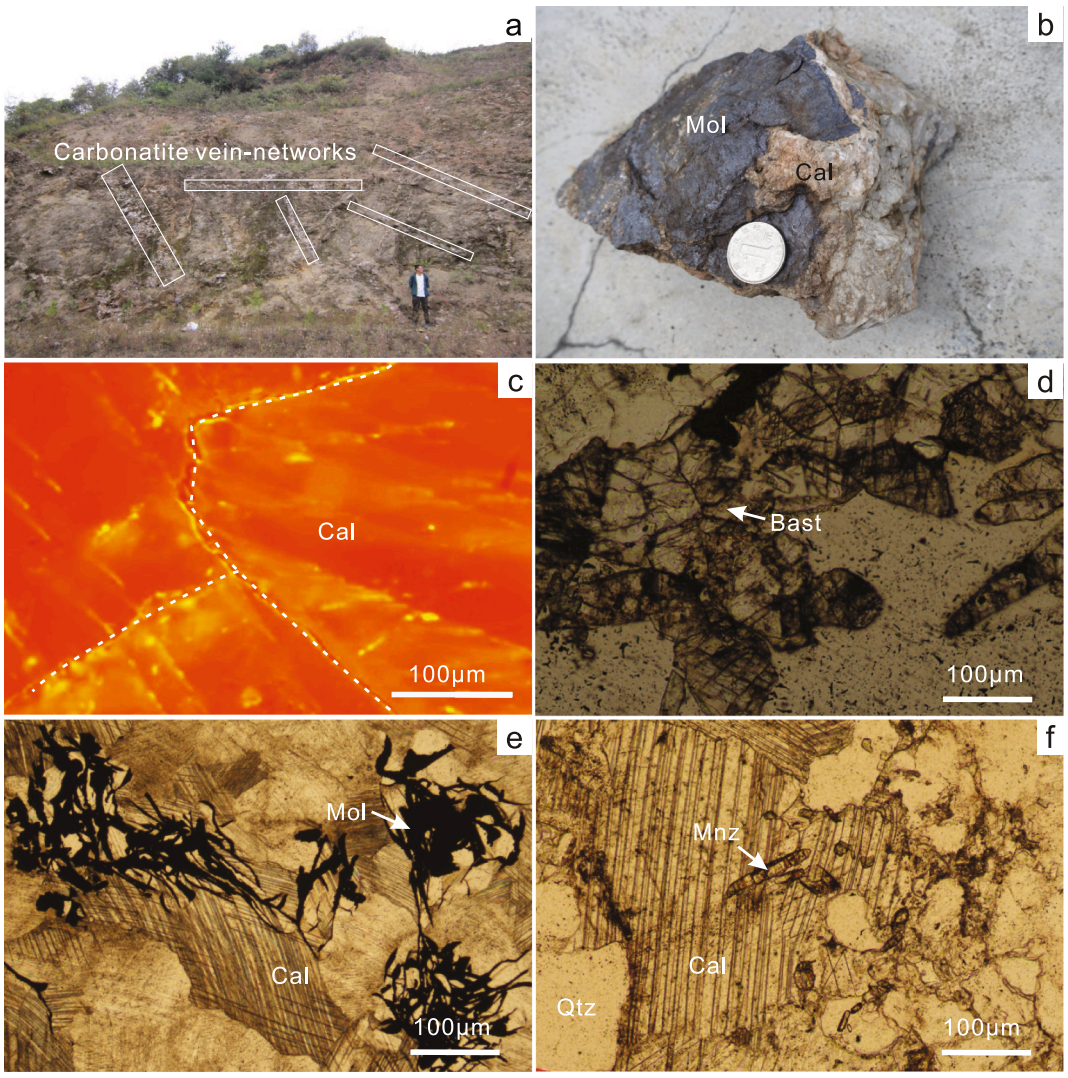

Fig. 2. (a) Field photo showing the stockwork carbonatite is about 10–50 m long with a width of about 0.1–1.5 m. (b) Photo of hand specimen showing molybdenite is closely associated with pink calcite carbonatites. (c) Cathodoluminescence image of calcite. (d–f) Micro-photos of minerals. Mol–molybdenite; Cal–calcite; Bast–bastnaesite; Mnz–monazite; Qtz–quartz. (For interpretation of the references to color in this figure legend, the reader is referred to the web version of this article.)

(Stein et al., 1997; Song et al., 2015a; Song et al., 2016; Zhang et al., 2019a,b).

3. Analytical methods

3.1. Calcite compositional analyses

Calcite separates were hand-picked from the Huanglongpu carbonatites. Major and trace element analyses of calcite separates from the Huanglongpu carbonatites were carried out at the State Key Laboratory of Isotope Geochemistry, Guangzhou Institute of Geochemistry, Chinese Academy of Sciences (GIGCAS). Fresh calcite separates were handpicked and then grounded to 200 mesh. Sample powder of Ca. 50 mg was fluxed with $LiBO_2$ to make homogeneous glass disks for ZSX 100e X-Ray Fluorescence (XRF) analyses. Loss on ignition (LOI) was obtained by determining the weight loss of samples ignited in a furnace at 900 °C for 2 h and allowed to cool in a desiccator to minimize moisture absorption, which can be a major error source in carbonate LOI determination. The trace elements were measured by the Thermo Scientific iCAP RQ ICP-MS with the rock standard of W-2a. Prior to the analysis, 50 mg of rock powder were dissolved in a Teflon bomb using 1 ml of HF (38%) and 0.5 ml of HNO_3 (68%). The sealed bomb was placed in an electric oven and heated to 190 °C for 24 h. The cooling solution was spiked with 1 ml of 1 μg ml^{-1} Rh, used as an internal standard, and evaporated on a hot plate. This was followed by 2 cycles of dilution with 1 ml of HNO_3 and evaporation to dryness. The final residue was re-dissolved in 8 ml of HNO_3. The bomb was re-sealed, returned to the oven and heated to 110 °C for 3 h. The final solution was diluted to 100 ml by addition of distilled de-ionized water for ICP-MS analysis. Duplicate analyses of samples and rock standards suggest the analytical accuracy is better than 95%.

3.2. Calcite C-O-Sr-Nd-Pb isotopic analyses

About 20 mg calcite powders were firstly treated with 100% phosphoric acid in a vacuum. The liberated CO_2 gas was collected for C–O isotopes analyses. C–O stable isotopic analyses were carried out on a VG IsoPrime II mass spectrometer at the State Key Laboratory of Isotope Geochemistry, GIGCAS. Analytical uncertainties are better than 0.08% for $\delta^{18}O$ (reported relative to SMOW) and 0.05% for $\delta^{13}C$ (relative to PDB).

Isotopic measurement was performed on the Neptune Plus multiple collector inductively coupled plasma mass spectrometry at the State Key Laboratory of Isotope Geochemistry, GIGCAS. For Sr–Nd–Pb isotope

Table 1
Major and trace elements composition of calcite from the Huanglongpu (HL) carbonatite.

Sample no.	18HL-2a	18HL-3	18HL-5a	18HL-5b	18HL-7	18HL-9a	18HL-11	19HL-2	19HL-4	19HL-6	19HL-7	19HL-15	19HL-24	19HL-28
Major element (wt %)														
CaO		51.67	52.32	52.34	53.25	51.87	53.34	52.89	53.10	52.74	51.33	52.56	53.25	53.24
MnO		2.76	3.25	3.10	2.52	2.70	2.50	2.79	1.89	2.49	2.49	2.37	2.45	2.43
SrO		0.58	0.56	0.56	0.59	0.71	1.01	0.81	0.95	0.69	0.63	0.74	0.79	0.78
Al2O3		0.61	0.13	0.43	0.30	0.80	0.28	0.08	0.06	0.06	0.62	0.06	0.06	0.06
MgO		0.39	0.49	0.41	0.36	0.37	0.40	0.58	0.44	0.59	0.64	0.61	0.59	0.59
Na2O		0.21	0.38	0.18	0.23	0.21	0.20	0.03	0.03	0.02	0.03	0.03	0.03	0.03
BaO		0.07	0.03	0.05	0.05	0.13	0.51							
Fe2O3T		0.16	0.10	0.10	0.19	0.18	0.17	0.30	0.37	0.46	0.55	0.54	0.47	0.49
TiO2		0.02	0.02	0.02	0.03	0.02	0.03	BD[a]	BD[a]	BD[a]	BD[a]	BD[a]	BD[a]	BD[a]
SiO2		0.91	BD[a]	BD[a]	BD[a]	0.61	0.28	0.31	1.01	0.11	2.15	0.48	BD[a]	0.05
P2O5		0.02	BD[a]	0.03	0.01	0.03	0.03	0.01	0.02	0.01	0.01	BD[a]	BD[a]	0.01
K2O		BD[a]	BD[a]	BD[a]	BD[a]	BD[a]	BD[a]	0.02	0.02	0.02	0.54	0.02	0.02	0.02
LOI		42.05	42.25	42.29	42.24	41.86	41.39	42.06	41.75	42.33	40.86	42.10	42.26	42.23
Total		99.44	99.53	99.50	99.78	99.49	100.13	99.89	99.64	99.51	99.85	99.50	99.88	99.92
Trace element (ppm)														
Li	0.27	0.16	0.09	0.29	0.08	0.14	0.11	0.16	0.14	0.23	0.24	0.30	0.11	0.10
Be	0.36	0.03	0.02	0.15	0.02	0.02	0.09	0.89	0.20	0.03	0.27	0.17	0.04	0.05
Mg	2900	2810	3130	2840	2650	2760	2720	2980	2070	3070	3340	3160	2970	3010
P	104.0	130.0	68.6	182.0	87.0	138.0	112.0	62.4	116	41.2	76.2	45.7	42.3	65.9
Sc	4.78	3.15	2.73	3.06	2.40	2.84	3.13	4.96	1.52	3.46	4.87	2.71	2.27	2.13
Trace element (ppm)														
Ti	3.66	3.64	1.24	1.56	5.81	4.00	2.42	1.93	2.45	1.38	2.69	1.98	2.15	1.21
V	1.36	0.41	0.26	0.48	0.36	0.39	0.45	0.34	0.36	0.22	0.39	0.14	0.22	0.20
Cr	95.50	12.40	3.06	7.65	15.10	6.83	10.50	9.05	9.36	7.00	6.11	0.08	8.42	0.11
Mn	21,900	18,800	22,200	21,000	17,000	18,400	16,700	21,000	14,600	19,400	19,800	18,900	18,600	18,700
Fe	5710	4260	3890	3900	4570	4360	4000	3150	3320	4520	5190	5040	4480	4540
Co	1.13	0.19	0.10	0.14	0.22	0.13	0.17	0.16	0.14	0.12	0.13	0.07	0.15	0.06
Ni	41.90	5.22	1.39	3.29	6.64	3.02	4.56	4.16	4.35	3.13	2.77	0.11	3.84	0.12
Cu	2.11	0.30	0.10	0.21	0.37	0.19	0.24	0.20	0.36	0.17	0.17	0.07	0.27	0.05
Zn	22.4	12.1	11.4	12.4	11.7	30.7	14.3	11.1	13.0	12.1	12.4	11.9	10.9	13.3
Rb	14.10	0.64	0.81	0.85	0.60	0.64	0.61	0.71	0.57	0.74	1.72	0.96	0.91	0.82
Sr	4810	7340	7080	7080	7670	9230	11,900	6520	7810	5630	5270	6320	6520	6400
Y	648	419	583	586	423	421	350	485	384	469	404	635	712	661
Zr	0.16	0.08	0.11	0.11	0.09	0.09	0.06	0.09	0.10	0.10	1.88	0.12	2.12	0.13
Nb	0.75	4.67	0.08	0.41	8.51	4.16	2.15	0.41	0.62	0.86	1.30	0.80	0.61	0.66
Mo	114.00	62.20	8.92	7.70	6.31	62.40	21.60	17.10	13.30	1.80	48.20	4.15	0.56	1.41
Sn	0.09	0.05	0.02	0.02	0.09	0.06	0.04	0.04	0.07	0.04	0.04	0.05	0.05	0.03
Cs	0.11	0.01	0.02	0.03	0.01	0.01	0.01	0.01	0.02	0.05	0.03	0.05	0.02	0.01
Ba	493	744	333	742	677	1800	5710	468	613	232	1360	573	225	193
La	198	438	282	958	285	538	393	307	492	143	201	133	157	215
Trace element (ppm)														
Ce	433	959	754	1990	711	1180	811	745	1160	386	427	361	421	559
Pr	54.3	114.0	103.0	229.0	93.3	142.0	98.1	97.2	145.0	53.8	51.2	51.8	59.6	76.6
Nd	229	441	449	863	387	543	385	404	579	241	205	241	272	340
Sm	59.6	78.4	98.4	143.0	79.0	95.9	71.7	82.6	103.0	62.2	45.6	66.6	70.4	84.0
Eu	16.9	19.4	25.1	32.9	20.0	23.1	18.1	21.4	24.2	17.1	12.6	19.0	19.9	22.7
Gd	66.1	72.0	89.8	125.0	70.2	83.1	63.5	77.8	88.3	62.5	48.6	70.8	73.5	83.2
Tb	11.30	9.48	12.90	15.20	9.84	10.80	8.47	11.10	11.10	10.10	7.90	12.00	12.30	13.30
Dy	73.20	52.80	72.60	79.20	54.70	57.60	46.50	63.10	57.20	60.30	48.30	73.70	77.10	78.70
Ho	17.50	11.70	15.80	17.00	11.90	12.20	9.89	14.30	12.20	13.50	11.60	17.20	18.10	17.80
Er	58.10	36.70	49.00	51.50	36.60	37.30	30.40	45.80	37.00	42.60	38.60	56.30	61.50	56.90
Tm	10.70	6.20	8.31	8.57	6.04	6.12	5.05	8.00	6.13	7.58	6.99	10.20	10.90	10.10
Yb	76.90	41.20	56.00	56.70	40.10	40.40	33.00	53.40	40.70	50.9	49.50	69.80	74.10	67.50
Lu	12	6.29	8.41	8.52	6.01	6.08	5.06	8.04	6.13	7.74	7.99	10.40	10.80	9.92
Hf	0.20	0.15	0.20	0.22	0.15	0.16	0.13	0.20	0.18	0.19	0.17	0.23	0.26	0.24
Ta	0.05	0.04	0.05	0.06	0.04	0.04	0.03	0.05	0.05	0.05	0.04	0.07	0.07	0.07
Pb	117	71.10	78.60	102	84.10	89.90	96.80	58	72.50	77.90	70.40	79.90	71.00	77.80
Th	1.21	3.32	0.23	2.64	1.63	3.14	3.46	0.72	1.44	0.44	1.51	0.15	0.25	0.60
U	6.10	4.50	0.10	0.54	7.29	3.82	1.84	0.60	1.01	0.61	0.83	0.59	0.37	0.27

[a] Below detection.

determination, sample powders were firstly dissolved in Teflon capsules with HF + HNO_3 acid. Strontium and REE were separated using cation columns, and then the Nd fractions were further separated using HDEHP-coated columns. For Pb isotope, the total procedural blank was less than 0.4 ng. Samples were doped with Tl, and mass discrimination was corrected using a certified $^{203}Tl/^{205}Tl$ ratio of 0.418922. During the period of analysis, repeated analyses of National Institute of Standards and Technology Standard Reference Material 981 yielded $^{206}Pb/^{204}Pb = 16.9325 \pm 5$ (2σ), $^{207}Pb/^{204}Pb = 15.4859 \pm 6$ (2σ), and $^{208}Pb/^{204}Pb = 36.6825 \pm 18$ (2σ). Measured $^{87}Sr/^{86}Sr$ and $^{143}Nd/^{144}Nd$ ratios were

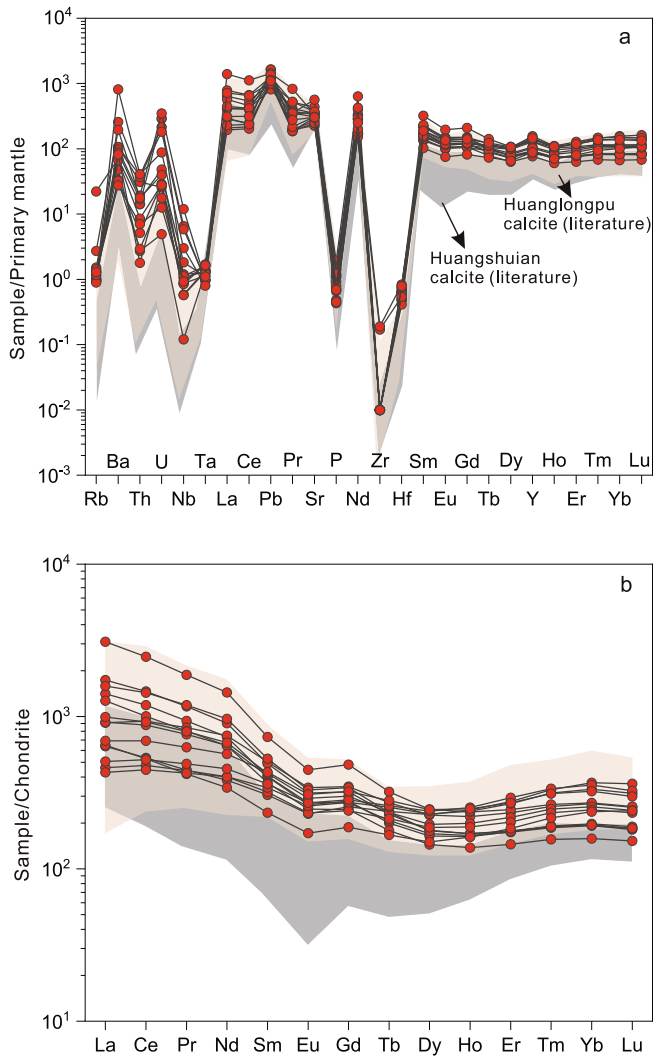

Fig. 3. (a) Primitive mantle-normalized trace-element abundances in calcite samples of carbonatites from Huanglongpu; (b) Chondrite-normalized REE abundances of calcite in Huanglongpu. Normalization values are from McDonough and Sun (1995). Huanglongpu and Huangshuian calcite (Bai et al., 2019) from the Qinling orogenic belt are also plotted for comparison.

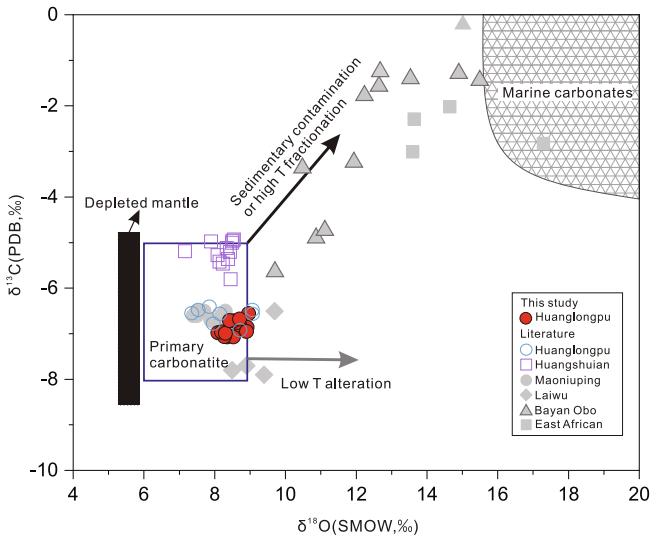

Fig. 4. Carbon and oxygen isotopic compositions of calcite from the Huanglongpu carbonatite. The field of primary, unmodified carbonatites (after Taylor et al., 1967) and the major processes responsible for changes in C–O isotopic composition of carbonatites (Demény et al., 1998) are also shown for comparison. Recycled sediments data from Moecher et al. (1994) and Eiler et al. (2000). MORB data from Eiler et al. (2000) and Deines. (2002).

normalized to $^{86}Sr/^{88}Sr = 0.1194$ and $^{146}Nd/^{144}Nd = 0.7219$, respectively. The reported $^{87}Sr/^{86}Sr$ and $^{143}Nd/^{144}Nd$ ratios were respectively adjusted to the NBS SRM 987 standard with an $^{87}Sr/^{86}Sr$ value of 0.71025 and the Shin Etsu JNdi-1 standard with a $^{143}Nd/^{144}Nd$ value of 0.512115.

4. Results

4.1. Elemental geochemistry

The major and trace elemental data of calcite separates from the Huanglongpu carbonatite are presented in Table 1 and illustrated in Fig. 3. The calcite has relatively higher MnO (1.9–3.2 wt%) and MgO (0.36–0.64 wt%) contents than calcite of other carbonatites in Lesser Qinling. It is enriched in large ion lithophile elements (Sr, Ba, Pb and U) but depleted in high field strength elements (Nb, Ta, Zr and Hf), which is similar to the average calcite compositions in most carbonatites (Fig. 3a, Castor, 2008; Lai and Yang, 2013; Stoppa et al., 2019). Total REE contents range from 1566 to 3196 ppm, consistent with those of igneous carbonatites (Samoilov, 1991; Mitchell, 2005). Notably, the Huanglongpu calcite is relatively enriched in the HREE with LREE/HREE ratios of 0.9–4.4 (Fig. 3b). REE distribution patterns of the Huanglongpu calcite are flatter with slightly negative Eu anomalies, when compared to calcite of the other carbonatites in the Qinling orogen (Fig. 3b, Bai et al., 2019). Moreover, the Huanglongpu calcite is more enriched in Pb (81 ppm on average) than the average calcite in the typical carbonatites.

4.2. Isotopic geochemistry

Carbon and oxygen isotopic data of the calcite samples are listed in Table 2 and illustrated on Fig. 4. $\delta^{13}C_{V\text{-}PDB}$ and $\delta^{18}O_{V\text{-}SMOW}$ values of the fourteen samples vary from −7.07‰ to −6.56‰ (−6.87‰ on average) and from 8.09‰ to 8.96‰ (8.54‰ on average), respectively. These uniform C–O isotopic data are plotted within the primary carbonatite domain (Fig. 4).

The Sr, Nd and Pb isotopic data are listed in Table 3 and illustrated on Fig. 5. The carbonatites have εNd(t) values (calculated at 220 Ma) of −8.03–−5.05, significantly lower than EM1 (Fig. 5a), and have $(^{87}Sr/^{86}Sr)_i$ values of 0.7049–0.7056, slightly lower than those of the EM1. They have $^{206}Pb/^{204}Pb$, $^{207}Pb/^{204}Pb$ and $^{208}Pb/^{204}Pb$ compositions ranging from 17.440 to 17.756, 15.441 to 15.481 and 37.540 to 37.677, respectively (Table 3; Fig. 5c). These C-O-Sr-Nd-Pb isotopic

Table 2
C–O isotopic composition of calcite from the Huanglongpu (HL) carbonatite.

Samples	18HL-2a	18HL-3	18HL-5a	18HL-5b	18HL-7	18HL-9a	18HL-11	19HL-02	19HL-04	19HL-06	19HL-07	19HL-15	19HL-24	19HL-28
$\delta^{13}C_{PDB}$(‰0	−6.56	−6.98	−7.07	−7.07	−7.06	−6.96	−6.99	−6.86	−6.81	−6.75	−6.95	−6.72	−6.71	−6.68
$\delta^{18}O_{SMOW}$(‰ z)	8.96	8.09	8.35	8.53	8.27	8.19	8.30	8.91	8.70	8.64	8.90	8.53	8.42	8.70

$\delta^{18}O_{SMOW}$ (%) = 1.03091 × $\delta^{13}O_{PDB}$ (%) + 30.91, according to Coplen et al. (1983).

Table 3
Sr − Nd − Pb isotopic composition of calcite from the Huanglongpu (HL) carbonatite.

Samples	$^{87}Rb/^{86}Sr$	$^{87}Sr/^{86}Sr$	2σ	$(^{87}Sr/^{86}Sr)_i$	$^{147}Sm/^{144}Nd$	$^{143}Nd/^{144}Nd$	2σ	$(^{143}Nd/^{144}Nd)_i$	εNd (t)	$^{206}Pb/^{204}Pb$	$^{207}Pb/^{204}Pb$	$^{208}Pb/^{204}Pb$	$(^{206}Pb/^{204}Pb)_i$	$(^{207}Pb/^{204}Pb)_i$	$(^{208}Pb/^{204}Pb)_i$
18HL-3	0.0003	0.705068	0.000004	0.705067	0.107464	0.512105	0.000003	0.511950	−7.88	17.713	15.448	37.573	17.577	15.441	37.540
18HL-5a	0.0003	0.705003	0.000003	0.705002	0.132476	0.512139	0.000003	0.511947	−7.93	17.458	15.471	37.643	17.455	15.471	37.641
18HL-5b	0.0003	0.705011	0.000004	0.705010	0.100165	0.512169	0.000003	0.512024	−6.43	17.480	15.471	37.675	17.468	15.470	37.657
18HL-7	0.0002	0.705011	0.000005	0.705010	0.123399	0.512225	0.000003	0.512047	−5.99	17.944	15.485	37.637	17.756	15.476	37.624
18HL-9a	0.0002	0.704946	0.000005	0.704945	0.106760	0.512174	0.000003	0.512020	−6.51	17.760	15.486	37.683	17.668	15.481	37.659
18HL-11	0.0001	0.704930	0.000004	0.704930	0.112578	0.512199	0.000003	0.512036	−6.20	17.540	15.473	37.683	17.499	15.471	37.658
19HL-02	0.0003	0.705049	0.000010	0.705048	0.123591	0.512121	0.000004	0.511942	−8.03	17.471	15.459	37.591	17.449	15.458	37.582
19HL-04	0.0002	0.704896	0.000008	0.704895	0.107536	0.512225	0.000004	0.512070	−5.54	17.510	15.471	37.641	17.480	15.469	37.627
19HL-06	0.0004	0.705298	0.000008	0.705297	0.156019	0.512321	0.000004	0.512095	−5.05	17.482	15.471	37.681	17.466	15.470	37.677
19HL-07	0.0009	0.705447	0.000010	0.705444	0.134464	0.512204	0.000004	0.512009	−6.72	17.508	15.468	37.678	17.482	15.467	37.663
19HL-15	0.0004	0.705444	0.000008	0.705442	0.167056	0.512305	0.000005	0.512063	−5.67	17.456	15.461	37.654	17.440	15.460	37.653
19HL-24	0.0004	0.705522	0.000010	0.705521	0.156459	0.512249	0.000004	0.512023	−6.45	17.461	15.467	37.671	17.449	15.466	37.669
19HL-28	0.0004	0.705426	0.000009	0.705425	0.149349	0.512284	0.000005	0.512068	−5.58	17.473	15.468	37.677	17.465	15.468	37.671

[$(^{87}Rb/^{86}Sr)_{CHUR} = 0.0847$ (Mcculloch and Black, 1984); $(^{87}Sr/^{86}Sr)_{CHUR} = 0.7045$ (DePaolo, 1988); $(^{147}Sm/^{144}Nd)_{CHUR} = 0.1967$ (Jacobsen and Wasserburg, 1980); $(^{143}Nd/^{144}Nd)_{CHUR} = 0.512638$ (Goldstein et al., 1984)] was used for the calculations. $\lambda_{Rb} = 1.42 \times 10^{-11}$ year^{-1}; $\lambda_{Sm} = 6.54 \times 10^{-12}$ year^{-1}. $(^{207}Pb/^{204}Pb)_{NHRL} = 0.1084 \times (^{206}Pb/^{204}Pb)_i + 13.491$; $(^{208}Pb/^{204}Pb)_{NHRL} = 1.209 \times (^{206}Pb/^{204}Pb)_i + 15.627$ (Hart, 1984). Initial Sr–Nd–Pb isotope ratios were obtained by using the age of 220 Ma.

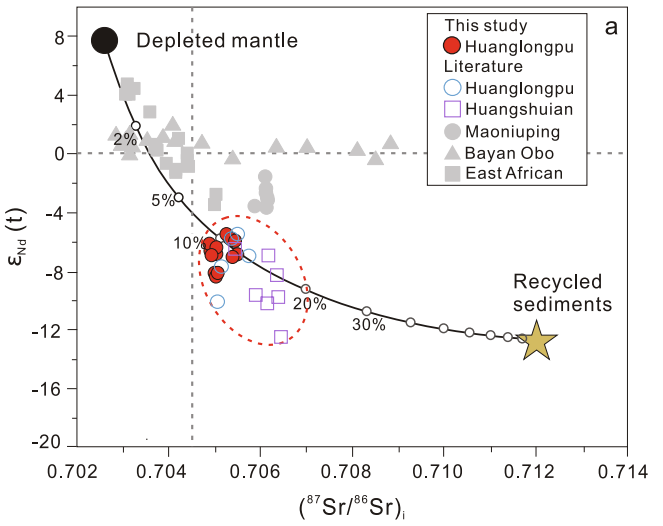

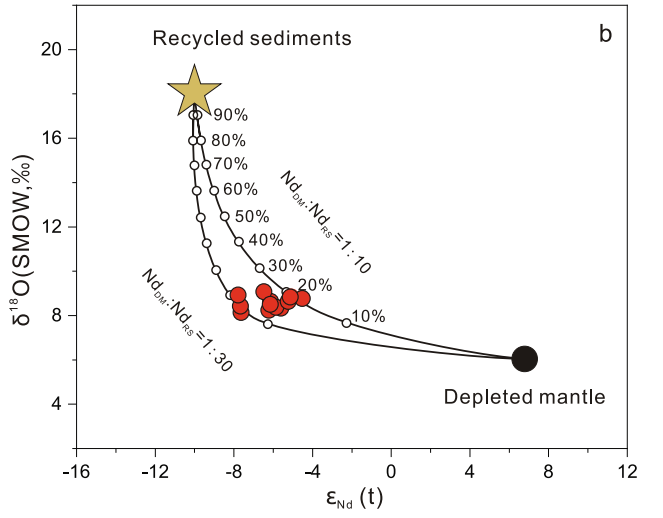

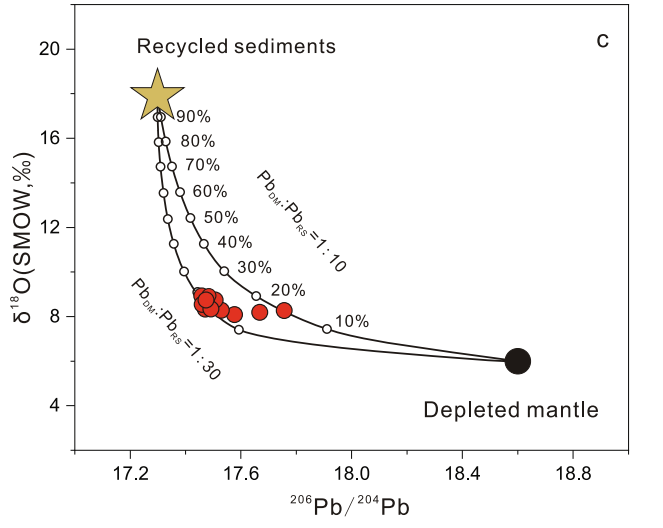

(caption on next column)

Fig. 5. (a) Modelling based on the Sr-Nd isotopic compositions to show the proportion of subducted sediments involved in the mantle area, (b) $\delta^{18}O$ versus εNd (t), and (c) $\delta^{18}O$ versus $^{206}Pb/^{204}Pb$. Recycled sediments data from Plank and Langmuir. (1998) and Eiler et al. (2000). Depleted mantle data from Eiler et al. (2000), Salters and Stracke, (2004) and Workman and Hart, 2005. Curve refer to simple mixing between the depleted mantle derived and recycled sediments. Parameters used as follows: Depleted mantle (DM): Sr = 8 ppm, Nd = 0.58 ppm, εNd = 7.8, and $^{87}Sr/^{86}Sr$ = 0.7026 (Salters and Stracke, 2004; Workman and Hart, 2005); and subducted sediments: Sr = 30 ppm, Nd = 12 ppm, εNd = −12, and $(^{87}Sr/^{86}Sr)_i$ = 0.7120 (Plank and Langmuir, 1998; Wang et al., 2012). The Maoniuping data from Hou et al. (2015). The Bayan Obo data from Yang et al. (2011). The East African data from Chikanda et al. (2019). And the Lesser Qinling data from Bai et al. (2019). Initial Sr-Nd-Pb isotope ratios were obtained by using the age of 220 Ma.

results are consistent with previous studies (e.g., Xu et al., 2010, 2011; Song et al., 2016; Smith et al., 2018; Bai et al., 2019).

5. Discussion

5.1. Geochemical affinity of the Huanglongpu calcite

The Huanglongpu carbonatite is a typical calcic-carbonatite, with 90 vol% calcite. In mineralogy, calcite in the Huanglongpu carbonatite vein-networks occurs as large-grained (0.1–1 mm in diameter) euhedral or subhedral crystal. It has uniform saffron color in cathodeluminescence image (Fig. 2c), indicating insignificant influence from late metasomatism or recrystallization (e.g., Pierson, 1981). Compositionally, the Huanglongpu calcite contains remarkably high contents of Sr, Ba and REE (Fig. 6a, b), which are obviously different from typical sedimentary and metamorphic calcite (e.g., Samoilov, 1991; Xu et al., 2007). Besides, the C–O isotopes fall within the primary carbonatite range, as well as the Maoniuping and Huanshuian carbonatite (Fig. 4), indicating the origin of mantle-derived melts. Accordingly, both compositional and isotopic data of calcite show that the Huanglongpu vein-networks were formed from igneous carbonatites that should be mantle-derived.

Previous experiments showed that calcio-carbonatite magma has a viscosity of 0.1 Pa·s and a density of 2.3–2.5 × 10^3 kg·m^{-3} at 700–800 °C, while the density of water-rich carbonatite is even lower, possibly less than 2 × 10^3 kg·m^{-3} (Wolff, 1994). Thus, such low density and viscosity allow the carbonatite magmas ascending rapidly after its formation (Dobson et al., 1996), preventing extensive wall-rock contamination. Besides, the relatively homogeneous Pb isotopic compositions and the absent of correlation between $^{87}Sr/^{86}Sr$ and Rb/Sr ratios of the Huanglongpu calcite further argue against significant crustal assimilation (Table 3). So, we conclude that the isotopic geochemistry of the Huanglongpu calcite should be mostly pristine and records the nature of the mantle source.

5.2. Nature of mantle source

Carbonatites are typical mantle-derived magmas (Woolley and Church, 2005; Bell and Simonetti, 2010). Previous studies have shown that most carbonatites have Sr-Nd-Pb isotopes similar to those of oceanic island basalts (OIBs) (e.g., Hou et al., 2015). Thus, these carbonatites were generally regarded to originate from partial melting of enriched sub-lithospheric mantle (Bell and Simonetti, 2010). In addition, some carbonatites were interpreted to originate from the deeper asthenospheric mantle modified by recycled crustal components (Bell and Simonetti, 2010). For the Huanglongpu carbonatites, the elevated HREE-enriched patterns are obviously different from those of OIBs, which are generally LREE-enriched (e.g., Eisele et al., 2002). In addition, the Nd isotope value (εNd(t) = −8.03–−5.05) of the Huanglongpu carbonatites are remarkably lower than those of OIBs when the Sr isotopes of carbonatites are the same to those of OIBs (e.g., Hofmann,

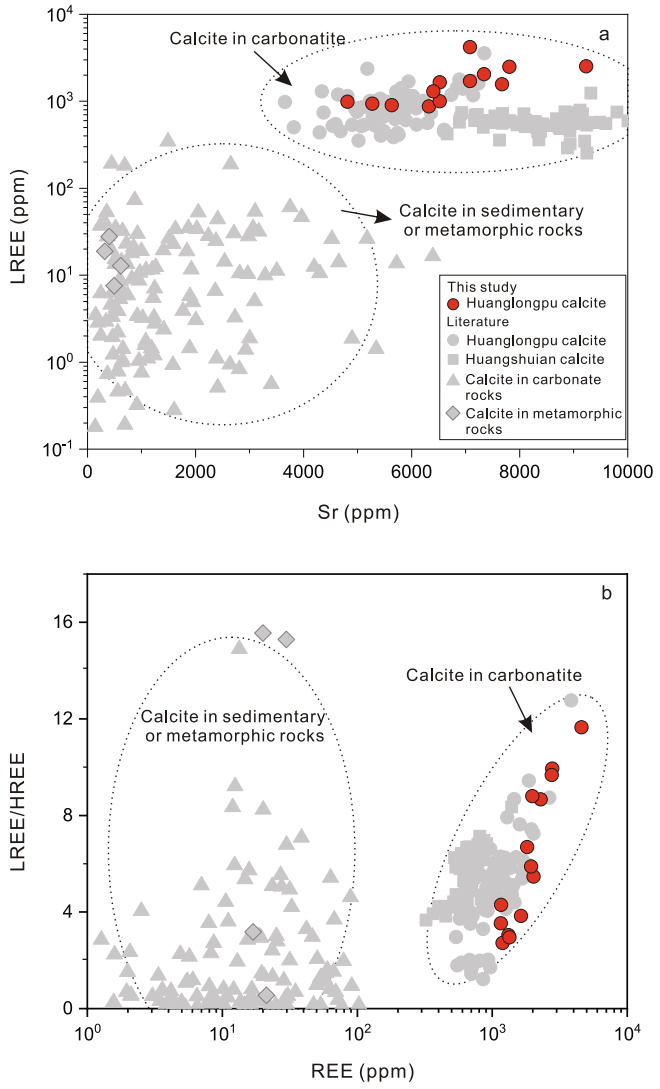

Fig. 6. (a) Sr versus LREE and (b) REE versus LREE/HREE for the Huanglongpu calcite. The Huanglongpu and Huangshuian calcite data from Bai et al. (2019). The calcite data of carbonate rocks from Xu et al. (2021). The calcite data of metamorphic rocks from Zhuo et al. (2019).

1997), suggesting that the Huanglongpu carbonatites cannot be generated by partial melting of enriched lithospheric mantle. Therefore, the source region of the Huanglongpu carbonatite may be an exotic hybridized mantle with recycled crustal material. In addition, the Pb isotopic compositions of the Huanglongpu carbonatites are also slightly higher than those of the depleted mantle, ascribed to the involvement of crustal materials (e.g., Salters and Stracke, 2004; Workman and Hart, 2005).

Carbonated mantle induced by recycle of marine sediments into the mantle is the favorable source of global carbonatites (e.g, Thomson et al., 2016; Plank and Manning, 2019). The residual carbonated eclogites formed after sediment melting and metamorphism are the main contributor to the carbon in the deep mantle (Dasgupta et al., 2004; Poli, 2016). In the Huanglongpu, the remarkable negative $\varepsilon_{Nd}(t)$ values and elevated initial $^{87}Sr/^{86}Sr$ ratios are distinctive with those of the Bayan Obo carbonatite, but partially overlap with those of the Maoniuping and East African carbonatites (Fig. 5a). Therefore, the contribution of subducted sediments is favored for the explanation of the mantle source of the Huanglongpu carbonatites rather than the lower continental crust. Besides, the melting of recycled sediments, which required considerable high temperature and pressure conditions (~1000 °C, ~3 GPa, Dokukina et al., 2017), calls for a slab window scenario induced by the upwelling of asthenosphere mantle. So, we infer that the hybrid mantle source should be mainly comprised of subducted sediments and surrounding depleted mantle. Mass-balance calculation by combining O-Sr-Nd-Pb isotopes can be used to constrain the contribution of subducted sediments and surrounding mantle source, as shown in Fig. 5. Sr-Nd isotopes show that the mantle sources of the Huanglongpu and Huangshuian carbonatites involve more than 10–20% recycled sediments (Fig. 5a). In addition, O-Nd and O-Pb isotopes give further supports for the contribution of 10–20% recycled sediments (Fig. 5b and c).

5.3. Contribution of recycled eclogite facies sediments

The Huanglongpu carbonatite is characterized by elevated HREE contents compared to global carbonatites (e.g., Xu et al., 2003; Xu et al., 2008; Chen et al., 2018; Zhang et al., 2019a,b). Several possible models can be attributed to the high HREE contents in carbonatites. Firstly, the liquid immiscibility from carbonate-silicate magmas has been suggested to account for the generation and the enrichment of REE in carbonatites (Veksler et al., 1998; Gudfinnsson and Presnall, 2005; Song et al., 2015b). Due to the distinct partition coefficients of La (~1.33) and Yb (~0.3) between carbonatite and silicate magmas (Veksler et al., 1998), liquid immiscibility can lead to the strong fractionation between HREE and LREE, leading the enrichment of LREE in carbonatites relative to HREE. Given that, the liquid immiscibility can be exclude for the formation of the HREE-rich Huanglongpu carbonatites. Secondly, redistribution of REE during hydrothermal alteration could lead to the enrichment of HREE in carbonatites, due to the different stability of REE-Cl^-, F^- or CO_3^{2-} complexes (e.g., Smith et al., 2018; Cangelosi et al., 2019). This possibility is can be excluded due to the in significantly hydrothermal metasomatism in the Huanglongpu carbonatites. Moreover, fractional crystallization could also lead to HREE enrichment in carbonatite. For example, the Malawi carbonatite retains a complete evolutionary process and are enriched in HREE in the late stage (Broomfendley et al., 2017; Chikanda et al., 2019). However, the lowest $(La/Yb)_N$ value of the Malawi carbonatite that has evolved to the late stage is 69.4 (Chikanda et al., 2019), which is still far lower than the HREE enrichment level of the Huanglongpu carbonatite ($(La/Yb)_N$ = 4.3–37.3, Bai et al., 2019). Accordingly, it is probably that the HREE

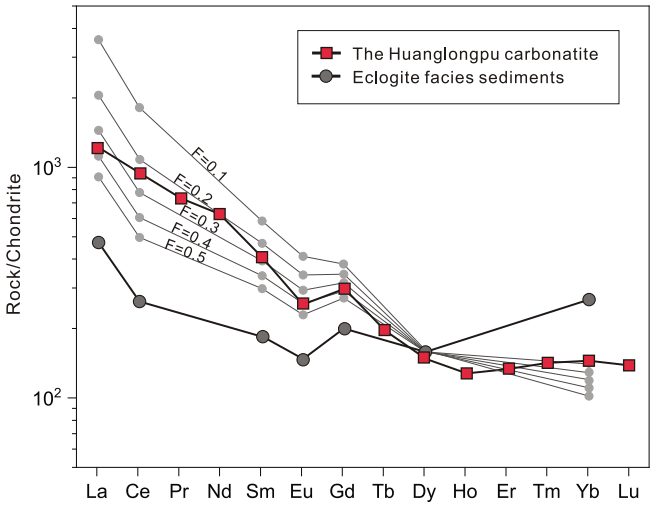

Fig. 7. Forward trace element modeling of incremental melting of an eclogite facies sediments source (40% clinopyroxene, 40% garnet, 10% olivine, 5% amphibole, 5% rutile) to generate the Huanglongpu carbonatites. F: mass percentage of melts. Normalization values are from McDonough and Sun (1995). Mineral-melt distribution coefficients are taken from the Chazot et al. (1996), Johnson, (1998), Westrenen et al. (1999), and Foley et al. (2000). The eclogite facies sediments (source rock) data are from Spandler et al. (2007).

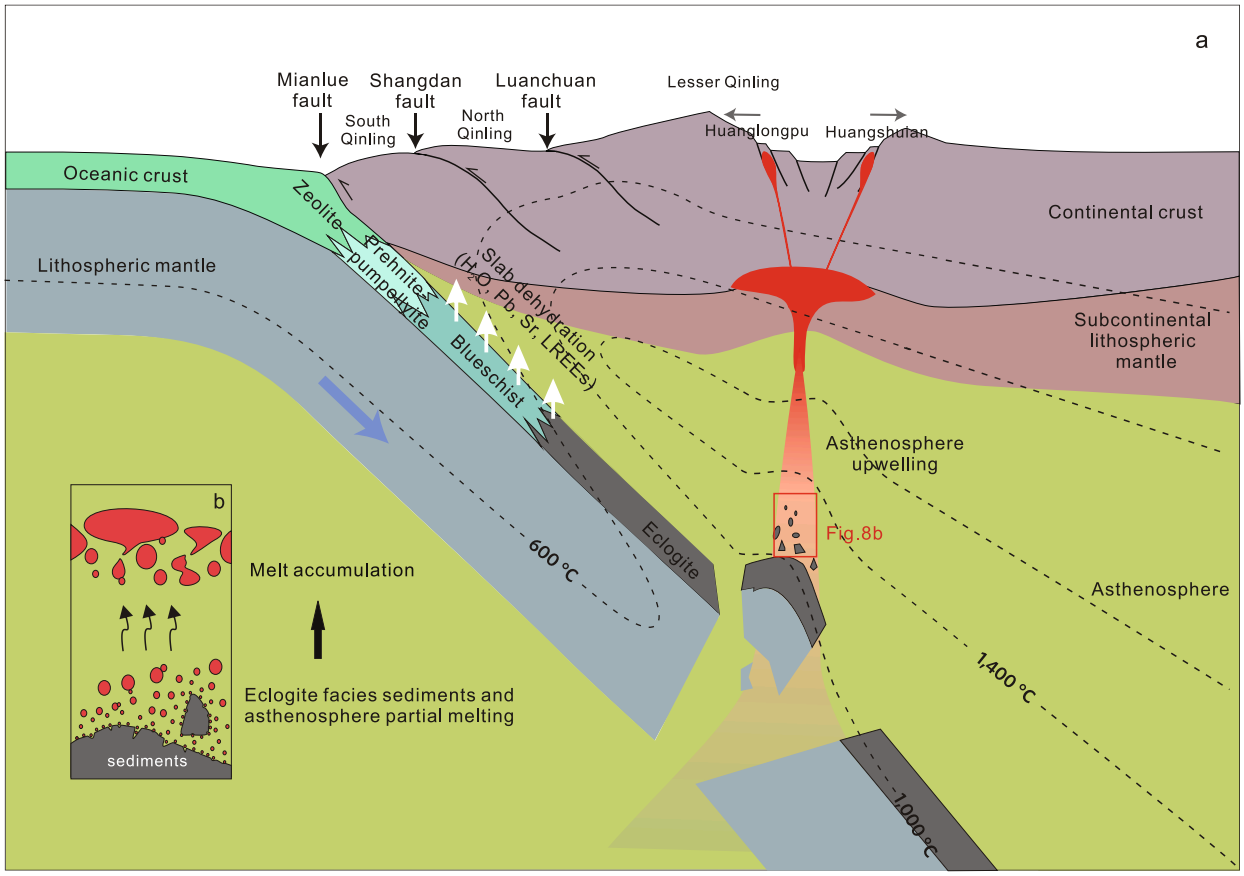

Fig. 8. Sketch maps for the formation of the Huanglongpu carbonatite. (a) The Mianlue oceanic slab subducted beneath the Lesser Qinling, where the recylced sediments got melted and mixed with the asthenosphere to form a hybridized source. The mantle source was partially melted to generate the primary magmas for the Huanglongpu carbonatite. The primary magmas upwelled under the post-orogenic extensional tectonic setting of the Lesser Qinling during the late Triassic, and eventually ascended along the fault to develop the Huanglongpu veined carbonatite. (b) The insert figure shows that the metamorphic eclogite facies sediments were partially melted to generate a CO_2, HREE and Mo enriched melts at ~ 1000 °C. The cartoon was modified from Wilkinson. (2013).

enrichment in the Huanglongpu carbonatite should be inherited from a HREE-enriched mantle source. Given that the depleted mantle has low REE abundances and partial melting of such a source cannot generate REE-rich melts (Salters and Stracke, 2004; Kogiso et al., 2004; Workman and Hart, 2005), such high REE concentration in the Huanglongpu carbonatites should be originated from the mantle source modified by the subducted sediments with HREE-bearing minerals (Plank and Langmuir, 1998; Wang et al., 2012; Bi et al., 2021).

When the oceanic slab subducted to the depth of ~ 50 km, the temperature and pressure can reach 1.4 GPa and 600 °C, respectively (Penniston-Dorland et al., 2015; Tsujimori and Mattinson, 2021). Under such conditions, the subducting slab with sediments could metamorphosed to eclogite facies (e.g., Tsujimori and Mattinson, 2021). Garnet and pyroxene are the main components in the eclogite and the garnet is the major host for HREE in the eclogite (Allibone et al., 2009; Clarke et al., 2013). The distribution coefficients between clinopyroxene and melts are experimentally determined to be $D^{cpx/melt}_{La} = 0.049$, $D^{cpx/melt}_{Gd} = 0.32$, and $D^{cpx/melt}_{Yb} = 0.4$, and the distribution coefficients between garnet and melts are $D^{gt/melt}_{La} = 0.004$, $D^{gt/melt}_{Gd} = 0.8$ and $D^{gt/melt}_{Yb} = 6.5$ (Johnson, 1998; Westrenen et al., 1999). Therefore, the partial melting of the eclogite facies sediments (~1000 °C, Putirka, 1998; Hammouda et al., 2009) could cause the MREE and HREE released from the garnet to the melts, and finally formed HREE-enriched carbonatites. The simulation results of partial melting of eclogite facies sedimentary rocks also show that the higher the degree of melting, the higher the HREE content in the melt (Fig. 7). Due to the low REE content of the depleted mantle ($\sum$REE = ~4.25 ppm), the REE pattern of the eclogite facies sediments melt can roughly represent the REE pattern of the source melt (Salters and Stracke, 2004). When the mass percentage of melts is ~ 0.3, the melts similar to the REE distribution pattern of the Huanglongpu carbonatite can be obtained. The HREE of the Huanglongpu carbonatite is slightly higher than the simulation result, which may be caused by subsequent magma differentiation. Our results indicate that the partial melting of eclogite facies sediments is the main cause for the enrichment of HREE in the Huanglongpu carbonatite.

5.4. Implications for Mo and HREE mineralization

Carbonatites are typically poor in Mo (~0.05 ppm) (Woolley and Kempe, 1989). However, the molybdenite in the Huanglongpu carbonatite is closely associated with calcite (Fig. 2e). Generally, the source of Mo can be evaluated by the Re contents in molybdenite (e.g., Mao et al., 1999; Xu et al., 2010). Molybdenite generated from mantle-derived melt/fluid is characterized by high Re contents (>100 ppm) and those with a crustal source show low Re contents (<10 ppm) (Mao et al., 1999). The Huanglongpu carbonatite-hosted molybdenite contains high Re contents (283–4000 ppm) (Huang et al., 1985; Xu et al., 2010), indicating a mantle origin. However, partial melting of the depleted mantle with very low Mo contents (0.02–0.6 ppm) is difficult to form the carbonatite with Mo mineralization (e.g., Salters and Stracke, 2004). Therefore, the enrichment of Mo in the mantle source may also be attributed to the addition of subducted materials. Previous studies have suggested that subduction sediments could be Mo-enriched with Mo contents up to 185 ppm, such as the black rock series (e.g., Plank and Langmuir, 1998; Wang et al., 2012). Such sediments input with subducted slab could account for Mo enrichment in the mantle source. This

hypothesis is also supported by the light Mo isotopic composition ($\delta^{98/95}$Mo value as low as −1.71‰ of the Huanglongpu carbonatite (authors' unpublished data). The $\delta^{98/95}$Mo value of the Huanglongpu carbonatite is markedly lower than those of sediments such as the black shales in Qinling ($\delta^{98/95}$Mo = −0.75‰ − 1‰) (Wen et al., 2011; Xu et al., 2012). Such low $\delta^{98/95}$Mo value may be due to the fact that the heavy Mo isotopes tend to migrate with the fluids to the overlying mantle wedge during the subduction process, leading to the low Mo isotopic compositions in the eclogite (König et al., 2016; Kendall et al., 2017). As with the subduction depth increases, the Mo isotopic value of the eclogite decreases (Chen et al., 2019). Therefore, the low Mo isotope values of the Huanglongpu carbonatite may be associated with the deep subduction process. As a result, the Mo mineralization of the Huanglongpu carbonatite is closely related to the recycled sediments.

A cartoon modeling showing the generation of the Huanglongpu carbonatite and the mechanisms of the Mo and HREE enrichment in the mantle source was illustrated in Fig. 8. In the Late Triassic, the Mianlue Ocean in the Qinling provided an opportunity for the sediment input, which brought large amount of Mo and HREE into the asthenosphere mantle (Dong and Santosh, 2016; Zhang et al., 2019a,b). During the early stages of oceanic subduction, the dehydrated fluids would have removed plenty of incompatible elements, such as LREEs from the slab, resulting in the HREE enrichment in the residues (Zheng, 2012; Zheng, 2019). These residues were subducted into deeper mantle and gradually metamorphosed into carbonated eclogites (Dasgupta et al., 2004; Poli, 2016; Thomson et al., 2016). In a subduction system under eclogite facies conditions, the minerals still maintain equilibrium in the solidus–liquidus interval (Sweeney, 1994). However, the Lesser Qinling was in a post-orogenic extensional tectonic setting in the Late Triassic (Dong and Santosh, 2016; Zhang et al., 2019a,b). The asthenosphere upwelling caused by the extensional collapse will carry the eclogite fragments and move upward. As the asthenosphere upwelling, the subducted materials begin to melt. When melting, the phase equilibrium of minerals is broken. In the MgO-CaO-SiO_2-CO_2 system (>1100 °C), magnesite and SiO_2 decompose to produce enstatite and CO_2, and supply CO_2 to carbonatite melts (Wyllie et al., 1983; Sleep and Zahnle, 2001). And the melting of Mo-bearing minerals (e.g., rutile) and HREE-bearing minerals (e.g., garnet and pyroxene) also contributes to Mo-HREE mineralization. Moreover, ongoing mechanical mixing leads to homogenization of the hybridized melt and further formation of the hybridized source (Fig. 8b). Due to the addition of subduction sediments in the source, the mantle source became rich in volatiles (Guzmics et al., 2008). The extensive accumulation of volatile components resulted in the fluidization of the carbonatite melts, which easily migrated upward into a shallow area. Eventually, the primary carbonatite magmas ascend along faults and formed a series of veins and mesh-veins of carbonatites associated with Mo-HREE mineralization.

6. Conclusions

The Huanglongpu carbonatites belongs to primary igneous carbonatites, derived from partial melting of eclogite facies sediments and the surrounding mantle. Sr-Nd, Nd-O and Pb-O isotope simulation results suggest that the mantle source of the carbonatites can be obtained through mixing of 10–20% subducted sediments and 80–90% depleted mantle. In addition, melting simulation of the eclogite facies sediments shows that the REE pattern of the Huanglongpu carbonatites could be obtained through 30% partial melting of the eclogite facies sediments. The sediments were recycled into the mantle by subduction and then hybridized with the depleted asthenosphere mantle under high temperature and pressure. Since eclogite facies sediments are also rich in Mo and HREE, this model provides a reasonable interpretation for the origin of the Huanglongpu Mo-HREE enrichment.

Declaration of Competing Interest

The authors declare that they have no known competing financial interests or personal relationships that could have appeared to influence the work reported in this paper.

Acknowledgments

This work was financially supported by the National Natural Science Foundation of China (41930424), the National Key R&D Program of China (2017YFC0602301) and the Science and Technology Planning Project of Guangdong Province, China (2020B1212060055). We are grateful to the constructive reviews from two anonymous reviewers and also the editorial work of Wei Terry Chen. We are also grateful to the help of Dr. Pan Qu, Ao Li, Zeyang Zhang and Qiang Weng for with isotopes analyses and helpful discussion. This is contribution No. IS-3084 from GIGCAS.

References

Allibone, A.H., Jongens, R., Turnbull, I.M., Milan, L.A., Daczko, N.R., De Paoli, M.C., et al., 2009. Plutonic rocks of western Fiordland, New Zealand: field relations, geochemistry, correlation and nomenclature. N. Z. J. Geol. Geophys. 52, 379–415.
Bai, T., Chen, W., Jiang, S.Y., 2019. Evolution of the carbonatite Mo-HREE deposits in the Lesser Qinling Orogen: insights from in situ geochemical investigation of calcite and sulfate. Ore Geol. Rev. 113, 103069.
Bell, K., Tilton, G.R., 2001. Nd, Pb and Sr isotopic compositions of east African carbonatites: evidence for mantle mixing and plume inhomogeneity. J. Petrol. 42, 1927–1945.
Bell, K., Simonetti, A., 2010. Source of parental melts to carbonatites-critical isotopic constraints. Mineral. Petrol. 98, 77–89.
Bell, K., Blenkinsop, J., Cole, T.J.S., Menagh, D.P., 1982. Evidence from Sr isotopes for long-lived heterogeneities in the upper mantle. Nature 298, 251–253.
Benkó, Z., Molnár, K., Magna, T., Rapprich, V., Palcsu, L., Pour, O., et al., 2021. Combined petrography, noble gas, stable isotope and fluid inclusion chemistry of carbonatites from Uganda: Implications for the origin of the carbonatite melt in continental rift setting. Chem. Geol. 578, 120213.
Bi, D.J., Shi, X.F., Huang, M., Yu, M., Zhou, T.C., Zhang, Y., et al., 2021. Geochemical and mineralogical characteristics of deep-sea sediments from the western North Pacific Ocean: constraints on the enrichment processes of rare earth elements. Ore Geol. Rev. 138, 104318.
Broomfendley, S., Brady, A.E., Wall, F., Gunn, G., Dawes, W., 2017. REE minerals at the Songwe Hill carbonatite, Malawi: HREE-enrichment in late-stage apatite. Ore Geol. Rev. 81, 23–41.
Cangelosi, D., Smith, M., Banks, D., Yardley, B., 2019. The role of sulfate-rich fluids in Heavy Rare Earth enrichment at the Dashigou carbonatite deposit, Huanglongpu, China. Mineral. Mag. 84, 1–51.
Castor, S.B., 2008. The Mountain Pass rare-earth carbonatite and associated ultrapotassic rocks, California. Canadian Mineral. 46, 779–806.
Chazot, G., Menzies, M.A., Harte, B., 1996. Determination of partition coefficients between apatite, clinopyroxene, amphibole, and melt in natural spinel lherzolites from Yemen: implications for wet melting of the lithospheric mantle. Geochim. Cosmochim. Acta 60, 423–437.
Chen, S., Hin, R.C., John, T., Brooker, R., Bryan, B., Niu, Y.L., et al., 2019. Molybdenum systematics of subducted crust record reactive fluid flow from underlying slab serpentine dehydration. Nat. Commun. 10, 4773.
Chen, W., Lu, J., Jiang, S.Y., Ying, Y.C., Liu, Y.S., 2018. Radiogenic Pb reservoir contributes to the rare earth element (REE) enrichment in South Qinling carbonatites. Chem. Geol. 494, 80–95.
Chen, Y.J., Santosh, M., 2014. Triassic tectonics and mineral systems in the Qinling Orogen, central China. Geol. J. 49, 338–358.
Chikanda, F., Otake, T., Ohtomo, Y., Ito, A., Yokoyama, T.D., Sato, T., 2019. Magmatic-hydrothermal processes associated with rare earth element enrichment in the Kangankunde Carbonatite Complex, Malawi. Minerals 9, 442.
Çimen, O., Kuebler, C., Simonetti, S.S., Corcoran, L., Mitchell, R., Simonetti, A., 2019. Combined boron, radiogenic (Nd, Pb, Sr), stable (C, O) isotopic and geochemical investigations of carbonatites from the Blue River Region, British Columbia (Canada): implications for mantle sources and recycling of crustal carbon. Chem. Geol. 529, 119240.
Clarke, G.L., Daczko, N.R., Miescher, D., 2013. Identifying Relic Igneous Garnet and Clinopyroxene in Eclogite and Granulite, Breaksea Orthogneiss, New Zealand. J. Petrol. 54, 1921–1938.
Coplen, T.B., Kendall, C., Hopple, J., 1983. Comparison of stable isotope reference samples. Nature 302, 236–238.
Dasgupta, R., Hirschmann, M.M., Withers, A.C., 2004. Deep global cycling of carbon constrained by the solidus of anhydrous, carbonated eclogite under upper mantle conditions. Earth Planet. Sci. Lett. 227, 73–85.
Deines, P., 2002. The carbon isotope geochemistry of mantle xenoliths. Earth Sci. Rev. 58, 247–278.

Demény, A., Ahijado, A., Casillas, R., Vennemann, T.W., 1998. Crustal contamination and fluid/rock interaction in the carbonatites of Fuerteventura Canary Islands, Spain: a C, O, H isotope study. Lithos 44, 101–115.
DePaolo, D.J., 1988. Neodymium Isotope Geochemistry: An Introduction. SpringerVerlag, Berlin.
Dobson, D.P., Jones, A.P., Rabe, R., Sekine, T., Kurita, K., Taniguchi, T., Kondo, T., Kato, T., Shimomura, O., Urakawa, S., 1996. In-situ measurement of viscosity and density of carbonate melts at high pressure. Earth Planet. Sci. Lett. 143, 207–215.
Dokukina, K.A., Mints, M.V., Konilov, A.N., 2017. Melting of eclogite facies sedimentary rocks in the Belomorian Eclogite Province, Russia. J. Metamorphic Geol. 35, 435–451.
Dong, Y.P., Santosh, M., 2016. Tectonic architecture and multiple orogeny of the Qinling Orogenic Belt, Central China. Gondwana Res. 29, 1–40.
Eiler, J.M., Schiano, P., Kitchen, N., Stolper, E.M., 2000. Oxygen-isotope evidence for recycled crust in the sources of mid-ocean-ridge basalts. Nature 403, 530–534.
Eisele, J., Sharma, M., Galer, S.J.G., Blichert-Toft, J., Devey, C.W., Hofmann, A.W., 2002. The role of sediment recycling in EM-1 inferred from Os, Pb, Hf, Nd, Sr isotope and trace element systematics of the Pitcairn hotspot. Earth Planet. Sci. Lett. 196, 197–212.
Fan, H.R., Hu, F.F., Yang, K.F., Wang, K.Y., 2006. Fluid unmixing/immiscibility as an ore-forming process in the giant REE-Nb-Fe deposit, Inner Mongolian, China: evidence from fluid inclusions. J. Geochem. Explor. 89, 104–107.
Foley, S.F., Barth, M.G., Jenner, G.A., 2000. Rutile/melt partition coefficients for trace elements and an assessment of the influence of rutile on the trace element characteristics of subduction zone magmas. Geochim. Cosmochim. Acta 64, 933–938.
Gerlach, D.C., Cliff, R.A., Davies, G.R., Norry, M., Hodgson, N., 1988. Magma sources of the Cape Verdes archipelago: isotopic and trace element constraints. Geochim. Cosmochim. Acta 52, 2979–2992.
Goldstein, S.L., Onions, R.K., Hamilton, P.J., 1984. A Sm–Nd isotopic study of atmospheric dusts and particulates from major river systems. Earth Planet. Sci. Lett. 70, 221–236.
Gudfinnsson, G.H., Presnall, D.C., 2005. Continuous gradations among primary carbonatitic, kimberlitic, melilititic, basaltic, picritic, and komatiitic melts in equilibrium with Garnet Lherzolite at 3–8 GPa. J. Petrol. 46, 1645–1659.
Guzmics, T., Zajacz, Z., Kodolányi, J., Werner, H., Szabó, C., 2008. LA-ICP-MS study of apatite- and K-feldsparhosted primary carbonatite melt inclusions in clinopyroxenite xenoliths from lamprophyres, Hungary: implication for significance of carbonatite melts in the Earth's mantle. Geochim. Cosmochim. Acta 72, 1864–1886.
Hammouda, T., Moine, B.N., Devidal, J.L., Vincent, C., 2009. Trace element partitioning during partial melting of carbonated eclogites. Phys. Earth Planet. Inter. 174, 60–69.
Hart, S.R., 1984. A large-scale isotope anomaly in the southernHemisphere mantle. Nature 309, 753–757.
Hofmann, A.W., 1997. Mantle geochemistry: the message from oceanic volcanism. Nature 385, 219–229.
Hou, Z.Q., Liu, Y., Tian, S.H., Yang, Z.M., Xie, Y.L., 2015. Formation of carbonatite-related giant rare-earth-element deposits by the recycling of marine sediments. Sci. Rep. 5, 1–10.
Huang, D.H., Wang, Y.C., Nie, F.J., Jiang, X.J., 1985. A new type of molybdenum deposit – geological characteristics and metal-logenic mechanism of the Huanglongpu carbonatite vein-type of molybdenum (lead) deposit, Shannxi. Acta Geol. Sin. 241–258 (In Chinese with English abstract).
Huang, D.H., Hou, Z.Q., Yang, Z.M., Li, Z.Q., Xu, D.X., 2009. Geological and geochemical characteristics, metallogenetic mechanism and tectonic setting of carbonatite vein-type Mo (Pb) deposits in the east qinling molybdenum ore belt. Acta Geol. Sin. 83, 1968–1984 (In Chinese with English abstract).
Jacobsen, S.B., Wasserburg, G.J., 1980. Sm–Nd isotopic evolution of chondrites. Earth Planet. Sci. Lett. 50, 139–155.
Johnson, K.T.M., 1998. Experimental determination of partition coefficients for rare earth and high-field-strength elements between clinopyroxene, garnet, and basaltic melt at high pressures. Contrib. Miner. Petrol. 133, 60–68.
Kalt, A., Hegner, E., Satir, M., 1997. Nd, Sr, and Pb isotopic evidence for diverse lithospheric mantle sources of East African Rift carbonatites. Tectonophysics 278, 31–45.
Kendall, B., Dahl, T.W., Anbar, A.D., 2017. The stable isotope geochemistry of molybdenum. Geochemistry 82, 683–732.
Kogiso, T., Hirschmann, M.M., Pertermann, M., 2004. High-pressure Partial Melting of Mafic Lithologies in the Mantle. J. Petrol. 45, 2407–2422.
König, S., Wille, M., Voegelin, A., Schoenberg, R., 2016. Molybdenum isotope systematics in subduction zones. Earth Planet. Sci. Lett. 447, 95–102.
Lai, X., Yang, X., 2013. Geochemical characteristics of the Bayan Obo giant REE–Nb–Fe deposit: constraints on its genesis. J. S. Am. Earth Sci. 41, 99–112.
Ling, M.X., Liu, Y.L., Williams, I.S., Teng, F.Z., Yang, X.Y., Ding, X., et al., 2013. Formation of the world's largest REE deposit through protracted fluxing of carbonatite by subduction-derived fluids. Sci. Rep. 3, 1776.
Liu, Y., Chakhmouradian, A.R., Hou, Z.Q., Song, W.L., Kynický, J., 2019. Development of REE mineralization in the giant Maoniuping deposit (Sichuan, China): insights from mineralogy, fluid inclusions, and trace-element geochemistry. Miner. Deposita 54, 701–718.
Lu, F.X., Zheng, J.P., Wang, F.Z., Sun, P., Liu, Y.S., Zhao, L., 1997. The comparison of constitution and thermal condition in North China Craton (NC), Yangtze Craton (YZ) and Qinling (QL) Orogenic Belt. Earth Sci. 3, 25–29.
Mao, J.W., Zhang, Z.C., Zhang, Z.H., Du, A.D., 1999. Re−Os isotopic dating of molybdenites in the Xiaoliugou W (Mo) deposit in the northern Qilian mountains and its geological significance. Geochim. Cosmochim. Acta 63, 1815–1818.
Mcculloch, M.T., Black, L.P., 1984. Sm–Nd isotopic systematics of ender by land granulites and evidence for the redistribution of Sm and Nd during metamorphism. Earth Planet. Sci. Lett. 71, 46–58.
Mitchell, R.H., 2005. Carbonatites and carbonatites and carbonatites. Can. Mineral. 43, 2049–2068.
Moecher, D.P., Valley, J.W., Essene, E.J., 1994. Extraction and carbon isotope analysis of CO2 from scapolite in deep crustal granulites and xenoliths. Geochim. Cosmochim. Acta 58, 959–967.
Penniston-Dorland, S.C., Kohn, M.J., Manning, C.E., 2015. The global range of subduction zone thermal structures from exhumed blueschists and eclogites: rocks are hotter than models. Earth Planet. Sci. Lett. 428, 243–254.
Pierson, B.J., 1981. The control of cathodoluminescence in dolomite by iron and manganese. Sedimentology 28, 601–610.
Plank, T., Langmuir, C.H., 1998. The chemical composition of subducting sediment and its consequences for the crust and mantle. Chem. Geol. 145, 325–394.
Plank, T., Manning, C.E., 2019. Subducting carbon. Nature 574, 343–352.
Poli, S., 2016. Melting carbonated epidote eclogites: carbonatites from subducting slabs. Prog. Earth Planet. Sci. 3.
Putirka, K., 1998. Garnet + liquid equilibrium. Contrib. Miner. Petrol. 131, 273–288.
Ratschbacher, L., Hacker, B.R., Calvert, A., Webb, L.E., Grimmer, J.C., McWilliams, M.O., et al., 2003. Tectonics of the Qinling (Central China): tectonostratigraphy, geochronology, and deformation history. Tectonophysics 366, 1–53.
Salters, V.J.M., Stracke, A., 2004. Composition of the depleted mantle. Geochem., Geophys., Geosyst. 5.
Samoilov, V.S., 1991. The main geochemical features of carbonatites. J. Geochem. Explor. 40, 251–262.
Sleep, N.H., Zahnle, K., 2001. Carbon dioxide cycling and implications for climate on ancient Earth. J. Geophys. Res. 106, 1373–1399.
Smith, M., Kynicky, J., Xu, C., Song, W., Spratt, J., Jeffries, T., et al., 2018. The Origin of secondary heavy Rare Earth Element enrichment in carbonatites: constraints from the evolution of the Huanglongpu district, China. Lithos 308, 787–789.
Song, W.L., Xu, C., Qi, L., Zhou, L., Wang, L.J., Kynicky, J., 2015a. Genesis of Si-rich carbonatites in Huanglongpu Mo deposit, Lesser Qinling orogen, China and significance for Mo mineralization. Ore Geol. Rev. 64, 756–765.
Song, W.L., Xu, C., Veksler, I.V., Kynicky, J., 2015b. Experimental study of REE, Ba, Sr, Mo and W partitioning between carbonatitic melt and aqueous fluid with implications for rare metal mineralization. Contrib. Miner. Petrol. 171, 1.
Song, W.L., Xu, C., Smith, M.P., Kynicky, J., Huang, K.J., Wei, C.W., et al., 2016. Origin of unusual HREE-Mo-rich carbonatites in the Qinling orogeny, China. Sci. Rep. 6, 37377.
Spandler, C., Mavrogenes, J., Hermann, J., 2007. Experimental constraints on element mobility from subducted sediments using high-P synthetic fluid/melt inclusions. Chem. Geol. 239, 228–249.
Stein, H.J., Markey, R.J., Morgan, J.W., Du, A., Sun, Y., 1997. Highly precise and accurate Re−Os ages for molybdenite from the East Qinling molybdenum belt, Shaanxi Province, China. Econ. Geol. 92, 827–835.
Stoppa, F., Schiazza, M., Rosatelli, G., Castorina, F., Sharygin, V.V., Ambrosio, F.A., et al., 2019. Italian carbonatite system: from mantle to ore-deposit. Ore Geol. Rev. 103041.
Sweeney, R., 1994. Carbonatite melt composition in the Earth's mantle. Earth Planet. Sci. Lett. 128, 259–270.
Taylor, H.P., Frechen, J., Degens, E.T., 1967. Oxygen and carbon isotope studies of carbonatites from the Laacher See District, West Germany and the Alno District, Sweden. Geochim. Cosmochim. Acta 31, 407–430.
Thomson, A.R., Walter, M.J., Kohn, S.C., Brooker, R.A., 2016. Slab melting as a barrier to deep carbon subduction. Nature 529, 76–79.
Tsujimori, T., Mattinson, C., 2021. Eclogites in Different Tectonic Settings. In: Alderton, D., Elias, S.A. (Eds.), Encyclopedia of Geology, Second Edition. Academic Press, Oxford, pp. 561–568.
Veksler, I.V., Petibon, C., Jenner, G.A., Dorfman, A.M., Dingwell, D.B., 1998. Trace element partitioning in immiscible silicate-carbonate liquid systems: an initial experimental study using a centrifuge autoclave. J. Petrol. 39, 2095–2104.
Wang, L.S., Zhang, F.X., Hou, J.F., Fang, B., Zhou, Y., 2012. Trace element geochemical characteristics of the Shuigoukou Formation black rock series in Shanyang area of the Qinling Mountains and their indication significance for sedimentation-mineralization. Geol. China 39, 311–325 (In Chinese with English abstract).
Wen, H.J., Carignan, J., Zhang, Y.X., Fan, H.F., Cloquet, C., Liu, S.R., 2011. Molybdenum isotopic records across the Precambrian – Cambrian boundary. Geology 39, 775–778.
Weng, Q., Yang, W.B., Niu, H.C., Li, N.B., Qu, P., Shan, Q., et al., 2021. B-Sr–Nd–Pb isotopic constraints on the origin of the Maoniuping alkaline syenite–carbonatite complex, SW China. Ore Geol. Rev. 135–104193.
Westrenen, W.V., Blundy, J., Wood, B., 1999. Crystal-chemical controls on trace element partitioning between garnet and anhydrous silicate melt. Am. Mineral. 84, 838–847.
Wolff, J.A., 1994. Physical properties of carbonatite magmas inferred from molten salt data, and application to extraction patterns from carbonatite-silicate magma chambers. Geol. Mag. 131, 145–153.
Woolley, A.R., Church, A.A., 2005. Extrusive carbonatites: a brief review. Lithos 85, 1–14.
Woolley, A.R., Kempe, D.R.C., 1989. Carbonatites: nomenclature, average chemical composition. In: Bell, K. (Ed.), Carbonatites: Genesis and Evolution. Unwin Hyman, London, pp. 1–14.
Workman, R.K., Hart, S.R., 2005. Major and trace element composition of the depleted MORB mantle (DMM). Earth Planet. Sci. Lett. 231, 53–72.
Wyllie, P.J., Huang, W.L., Otto, J., Byrnes, A.P., 1983. Carbonation of peridotites and decarbonation of siliceous dolomites represented in the system CaO-MgO-SiO_2-CO_2 to 30 kbar. Tectonophysics 100, 359–388.

Xu, R., Deng, M.G., Li, W.C., Lai, C.K., Zaw, K., Gao, Z.W., et al., 2021. Origin of the giant Luziyuan Zn-Pb-Fe(-Cu) distal skarn deposit, Baoshan block, SE Tibet: constraints from Pb–Sr isotopes, calcite C-O isotopes, trace elements and Sm–Nd dating. J. Asian Earth Sci. 205, 104587.
Xu, C., Huang, Z.L., Liu, C.Q., Qi, L., Li, W.B., Guan, T., 2003. Geochemistry of carbonatites in Maoniuping REE deposit, Sichuan province, China. Sci. China, Ser. D Earth Sci. 46, 246–256.
Xu, C., Campbell, I.H., Allen, C.M., Huang, Z.L., Qi, L., Zhang, H., et al., 2007. Flat rare earth element patterns as an indicator of cumulate processes in the Lesser Qinling carbonatites, China. Lithos 95, 267–278.
Xu, C., Campbell, I.H., Allen, C.M., Chen, Y.J., Huang, Z.L., Qi, L., et al., 2008. U-Pb zircon age, geochemical and isotopic characteristics of carbonatite and syenite complexes from the Shaxiongdong, China. Lithos 105, 118–128.
Xu, L.G., Lehmann, B., Mao, J.W., Nagler, T.F., Neubert, N., Bottcher, M.E., Escher, P., 2012. Mo isotope and trace element patterns of lower Cambrian black shales in South China: multi-proxy constraints on the paleoenvironment. Chem. Geol. 318, 45–59.
Xu, C., Song, W.L., Qi, L., Wang, L.J., 2009. Geochemical characteristics and tectonic setting of ore–bearing carbonatites in Huanglongpu Mo ore field. Acta Petrol. Sin. 25, 422–430 (In Chinese with English abstract).
Xu, C., Kynicky, J., Chakhmouradian, A.R., Qi, L., Song, W.L., 2010. A unique Mo deposit associated with carbonatites in the Qinling orogenic belt, central China. Lithos 118, 50–60.
Xu, C., Taylor, R.N., Kynicky, J., Chakhmouradian, A.R., Song, W., Wang, L., 2011. The origin of enriched mantle beneath North China block: evidence from young carbonatites. Lithos 127, 1–9.
Yang, K.F., Fan, H.R., Santosh, M., Hu, F.F., Wang, K.Y., 2011. Mesoproterozoic carbonatitic magmatism in the Bayan Obo deposit, Inner Mongolia, North China: constraints for the mechanism of super accumulation of rare earth elements. Ore Geol. Rev. 40, 122–131.
Zhang, G.W., Guo, A.L., Dong, Y.P., Yao, A.P., 2019b. Rethinking of the Qinling rogen. J. Geomech. 25 (5), 746–768.
Zhang, D.X., Liu, Y., Pan, J.Q., Dai, T.G., Bayless, R.C., 2019a. Mineralogical and geochemical characteristics of the Miaoya REE prospect, Qinling orogenic Belt, China: insights from Sr–Nd–C–O isotopes and LA-ICP-MS mineral chemistry. Ore Geol. Rev. 110, 102932.
Zheng, Y.F., 2012. Metamorphic chemical geodynamics in continental subduction zones. Chem. Geol. 328, 5–48.
Zheng, Y.F., 2019. Subduction zone geochemistry. Geosci. Front. 10 (4), 1223–1254.
Zhuo, Y.Z., Hu, R.Z., Xiao, J.F., Zhao, C.H., Huang, Y., Yan, J., et al., 2019. Trace elements and C-O isotopes of calcite from Carlin-type gold deposits in the Youjiang Basin, SW China: constraints on ore-forming fluid compositions and sources. Ore Geol. Rev. 113, 103067.